NeuroImage 290 (2024) 120562

Contents lists available at ScienceDirect

NeuroImage

journal homepage: www.elsevier.com/locate/ynimg

Stochastic brain dynamics exhibits differential regional distribution and maturation-related changes

Andrea Scarciglia [a,b,*], Vincenzo Catrambone [a,b], Martina Bianco [a,c], Claudio Bonanno [c], Nicola Toschi [d,e], Gaetano Valenza [a,b]

[a] Department of Information Engineering, School of Engineering, University of Pisa, Italy
[b] Bioengineering and Robotics Research Center E.Piaggio, School of Engineering, University of Pisa, Italy
[c] Department of Mathematics, University of Pisa, Italy
[d] Department of Biomedicine and Prevention, University of Rome "Tor Vergata", Rome, Italy
[e] A.A. Martinos Center for Biomedical Imaging, MGH and Harvard Medical School, Boston, MA, USA

ARTICLE INFO

Dataset link: http://www.humanconnectomeproject.org, https://camcan-archive.mrc-cbu.cam.ac.uk/dataaccess/, https://github.com/AndScar/noise_estimation

Keywords:
fMRI
Noise
Aging

ABSTRACT

Functional magnetic resonance imaging (fMRI) is a powerful non-invasive method for studying brain function by analyzing blood oxygenation level-dependent (BOLD) signals. These signals arise from intricate interplays of deterministic and stochastic biological elements. Quantifying the stochastic part is challenging due to its reliance on assumptions about the deterministic segment. We present a methodological framework to estimate intrinsic stochastic brain dynamics in fMRI data without assuming deterministic dynamics. Our approach utilizes Approximate Entropy and its behavior in noisy series to identify and characterize dynamical noise in unobservable fMRI dynamics. Applied to extensive fMRI datasets (645 Cam-CAN, 1086 Human Connectome Project subjects), we explore lifelong maturation of intrinsic brain noise. Findings indicate 10% to 60% of fMRI signal power is due to intrinsic stochastic brain elements, varying by age. These components demonstrate a physiological role of neural noise which shows a distinct distributions across brain regions and increase linearly during maturation.

1. Introduction

Functional magnetic resonance imaging (fMRI) is a powerful tool for measuring blood oxygenation level-dependent (BOLD) signals in the brain. However, these signals can be contaminated by various noise sources, which can be broadly divided into measurement noise and intrinsic brain noise (Krüger and Glover, 2001; Power et al., 2012; Liu, 2016). Measurement noise, sometimes referred to as additive or output noise, primarily originates from factors related to the scanner, such as thermal noise (Krüger and Glover, 2001), and artifacts caused by the subject's head motion (Power et al., 2012) or physiological fluctuations like cardiac and respiratory cycles (Birn et al., 2006). Given $y_n = x_n + \epsilon_n$, where y_n denotes the fMRI signal and x_n represents the intrinsic brain activity, measurement noise ϵ_n contributes to the system dynamics with a specific statistical distribution and power spectral density. Thermal noise is a fundamental noise source, arising from the random motion of electrons in the MRI system's receiver coil and other electronic components (Krüger and Glover, 2001). Other scanner-related noise sources include fluctuations in the fMRI signal due to scanner hardware, such as gradient coil heating, magnetic field instability, and RF coil imperfections (Krüger and Glover, 2001). Artifacts can also be introduced during fMRI data acquisition due to the subject's movement or physiological processes, including respiration, cardiac pulsation, and vasomotor activity (Birn et al., 2006). Furthermore, the relatively low sampling rate of fMRI data compared to these physiological processes can lead to aliasing of high-frequency signals, resulting in spurious low-frequency fluctuations (Lowe et al., 1998).

In contrast, intrinsic stochastic components in brain dynamics arise from the inherent variability and randomness of neuronal activity and inter-neuronal interactions (Fox et al., 2005; Deco et al., 2009a,b). Recent studies have underscored the pivotal role of stochastic neural network states (Destexhe and Contreras, 2006; Ponce-Alvarez et al., 2018), also highlighting the need for experimental paradigms and theoretical frameworks to comprehend noise dynamics at the brain network level. Stochastic changes in synaptic activities are believed to enhance neural network performance, potentially contributing to learning (Basalyga and Salinas, 2006). Moreover, the occurrence of information transfer at chemical synapses, where vesicles fuse with the plasma membrane and release neurotransmitter, is a stochastic process, and its likelihood of

* Corresponding author at: Department of Information Engineering, School of Engineering, University of Pisa, Italy.
E-mail address: andrea.scarciglia@phd.unipi.it (A. Scarciglia).

https://doi.org/10.1016/j.neuroimage.2024.120562
Received 16 November 2023; Received in revised form 29 February 2024; Accepted 1 March 2024
Available online 12 March 2024

occurrence plays a crucial role in regulating signal propagation within neuronal networks (Branco and Staras, 2009). Finally, stochastic resonance has been observed to enhance processing both in experimental and theoretical models of neural systems (McDonnell and Ward, 2011).

Intrinsic brain noise is dynamic since it is involved in brain activity over time. Specifically, it can be modeled as $y_n = T(y_{n-1}, y_{n-2}, \dots, y_0) + \varepsilon_n$, where y_n represents the fMRI signal at time t_n and $\{\varepsilon_n\}_n$ denotes the intrinsic brain noise. Characterizing $\{\varepsilon_n\}_n$ is crucial for ensuring the reliability and validity of fMRI-based inferences on brain function (Fox et al., 2007). However, determining whether a component is signal or noise depends on understanding the underlying physiology and biophysics (Liu, 2016). For example, components initially considered noise later became signals of significant interest (Liu, 2016). This is because estimating the dynamical brain noise $\{\varepsilon_n\}_n$ depends on the precise definition of the deterministic function T. Recent studies have focused on investigating the stochastic component in brain regions in relation to waveform regularity and orderliness, as explored by Hoffman et al. (2023). This study employ statistical comparisons to assess the expected waveform regularity. However, it is important to note that the waveform regularity approach assumes brain dynamics to be entirely random, without considering the potential presence of complex and possibly chaotic deterministic components in brain functioning. In this study, we address this limitation and quantify the intrinsic stochastic component in brain dynamics by measuring ε_n in fMRI signals without making assumptions about the deterministic function T. Our approach aims to provide an estimation technique applicable to any continuous and differentiable function underlying brain dynamics, as T may be specific to e.g. a particular brain region and/or a particular task. Here, we assume that in MRI measurement is not associated with age and explore whether age-related physiological changes in the brain are associated with modulation of estimates of intrinsic dynamical brain noise. To achieve this objective, we analyze stochastic brain components across different stages of brain maturation, leveraging high-quality publicly available fMRI datasets. We specifically utilize two publicly-available datasets: the Cam-CAN (Cambridge Centre for Ageing and Neuroscience) (Taylor et al., 2017) and the Human Connectome Project (HCP) (Van Essen et al., 2013). The Cam-CAN dataset, designed to explore shifts in cognitive abilities during healthy aging, provides comprehensive data, including functional MRI, from a population-based cohort of over 700 healthy individuals aged 18 to 87 years. In contrast, the HCP dataset aims to provide a comprehensive understanding of the structural and functional connectivity of the human brain. It includes high-resolution functional MRI data, along with other data types, from more than 1200 healthy young adults aged 22 to 35 years. Despite the narrower age range in the HCP dataset, it was selected for this investigation to offer additional insights into the modulation of intrinsic brain noise across different brain regions and age groups within a substantial data sample. Through the analysis of these datasets, we seek to gain a deeper understanding of the role of intrinsic brain noise in the context of healthy aging and brain function.

Numerous studies have shown that healthy aging is often linked to neurodegeneration (Chen, 2019), which manifests as changes in brain activity (Dennis and Thompson, 2014; Daselaar et al., 2006), as well as to reduced tissue volume, an accumulation of silent lesions, and increased iron deposits in multiple brain regions, particularly in subcortical areas (MacDonald and Pike, 2021). Recent studies have mechanistically linked healthy aging to white-matter degradation and dynamical compensation (Petkoski et al., 2023) as well as interhemispheric dedifferentiation (Lavanga et al., 2023). Previous fMRI research has identified lower activation in specific brain regions, such as the prefrontal cortex and hippocampus, in older adults during cognitive tasks involving memory and attention (Grady et al., 2000; Park et al., 2004). The frontoparietal network and its associated neural networks are more active in young individuals compared to elderly individuals during the resting state, attributed to a reduction in grey matter volume and white matter deterioration (Marstaller et al., 2015). Furthermore, white matter cerebrovascular reactivity responses are higher and faster in elderly subjects compared to grey matter (Thomas et al., 2014). A decline in cerebrovascular health and reduced cerebral blood flow in older adults have been observed, while accounting for concurrent age effects in brain volume (Lu et al., 2011; Tarumi et al., 2014; Chen et al., 2013) This phenomenon has been associated with both increasing arterial stiffness (Heffernan et al., 2008) and cognitive decline (Xekardaki et al., 2015). Conversely, some studies have observed increased activation in the aging brain, a phenomenon referred to as overactivation. This is believed to represent compensatory mechanisms that help maintain cognitive performance in the face of age-related neural decline (Cabeza, 2002; Reuter-Lorenz and Stanczak, 2000).

2. Materials and methods

2.1. Defining intrinsic brain noise

Let us consider the signal measured in a brain voxel as an observable generated by an unknown, discrete metric dynamical system (Y, μ, T). In this model, Y denotes a compact subset of $\mathbb{R}$, while T represents a differentiable mapping function with a bounded derivative that conserves the probability measure μ. Intuitively, the collected signal is generated by a deterministic, unknown and smooth function or map whose values are restricted to a limited interval of the real numbers. In this context, we assume that a noise-free fMRI signal from a voxel can be expressed as $w_n = T(w_{n-1}, w_{n-2}, \dots, w_0)$, where $w_i \in Y$ for all positive integers i.

We define the stochastic aspects of brain dynamics as a sequence of independent and identically distributed (IID) random variables $\{\varepsilon_n\}_n$, which form the *intrinsic dynamical brain noise*. The samples of ε_n alter the brain dynamics at each step, as outlined in the following equation:

$$y_n = T(y_{n-1}; y_0) + \varepsilon_n. \tag{1}$$

This equation may include generic mapping functions, such as $y_n = T(y_{n-1}, y_{n-2}, \dots, y_0) + \varepsilon_n$, where $y_i \in Y$ for all positive integers i, and $y(\varepsilon)_{n=1}^{N}$ represents a noisy fMRI time series containing N samples. We propose a method for estimating ε_n without any knowledge of the specific T function, applicable to any T function in the presence of measurement and dynamical noise. To the best of our knowledge, other techniques in the literature, like Kalman filter or the autoregressive models, are not able to analytically estimate noise ε_n without specific information or assumptions about the system dynamics equation T.

Let $x \to \psi(x)$ signify the Probability Density Function (PDF) of the random variable determined by the difference between any two samples of the noise process. For any output of the system, dynamically corrupted by noise according to the model $y(\varepsilon) = (y_0, T(y_0) + \varepsilon_1, T(T(y_0) + \varepsilon_1) + \varepsilon_2, \dots)$, the following holds (Scarciglia et al., 2023b):

$$\mathrm{ApEn}(y_n(\varepsilon)_{n=1}^{\infty}, m, r) \approx -\log\left[2\psi(0)r\right] \tag{2}$$

for any embedding dimension $m \in \mathbb{N}$ and for a sufficiently small tolerance r. Here, ApEn represents the nonlinear quantifier *Approximate Entropy*, which has been introduced by Pincus (1991) as a substitute of the exact regularity statistic *Kolmogorov–Sinai Entropy*, which measures the amount of information needed to describe any element, or equivalently, the possibility of finding repetitive or really close patterns of a time series. This index of regularity has been used to estimate the complexity of a system through the presence of regular patterns.

2.2. Estimation of intrinsic brain noise

Contrary to the Markovian framework, which models the fMRI signal at a specific time point as dependent on a limited number of prior time points and governed by transition probabilities between consecutive states, the quantitative approach proposed here does not assume full stochasticity nor the finite memory effects. In particular, the model assumes the following:

- Brain dynamics encompass both deterministic and stochastic components;
- The deterministic components of brain dynamics are regulated by any differentiable map T, potentially accounting for deterministic chaos (Scarciglia et al., 2023b);
- Random fluctuations of brain dynamics are realizations of IID Gaussian, stationary, random variables $\{\varepsilon_n\}_n$, following the distribution $\mathcal{N}(0,\sigma^2)$, excluding non-autonomicity for short recordings during the same state;
- The stochastic components of brain dynamics represent realizations of dynamical noise: for a noise sequence $\{\varepsilon_n\}_n \sim \mathcal{N}(0,\sigma^2)$, any fMRI signal assumes the form $y_n = T(y_{n-1},\dots,y_0)+\varepsilon_n$.

In the context of fMRI analysis, the properties of the map T are deemed highly versatile and suitable for describing and modeling a wide range of observable phenomena. Given these assumptions and following the theory in Section 2.1, Eq. (2) becomes:

$$\mathrm{ApEn}(\{y_n(\sigma)\}_{n=1}^{\infty}, m, r) \approx -\log\left[r/(\sigma\sqrt{\pi})\right]$$

As a result, we can infer the power σ of intrinsic brain noise in a closed form as follows:

$$\log(\sigma) \approx \mathrm{ApEn}(\{y_n(\sigma)\}_{n=1}^{\infty}, m, r) + \log(r/\sqrt{\pi})$$

where n denotes a time index, m represents the embedding dimension when $r < \sigma$ and $r \to 0^+$. In this case, the noise standard deviation σ can be approximated by the tolerance value r at which the functions $z \to \mathrm{ApEn}\left(\{y_n(\varepsilon)\}_{n=1}^{\infty}, m, z\right)$ and $z \to -\log z$ exhibit the most similar differential behavior, or the most similar slope.

By considering a noisy fMRI series $\{y_n(\varepsilon)\}_{n=1}^{N}$ comprising N samples, the estimation of intrinsic brain noise power σ^2 can be performed as follows. Set an embedding dimension m and estimate the profile map $r \to \mathrm{ApEn}(\{y_n(\varepsilon)\}_{n=1}^{N}, m, r)$ as a function of the tolerance parameter r, which ranges from 0 to the amplitude of the series $\{y_n(\varepsilon)\}_{n=1}^{N}$ with an arbitrary Δr step. An initial standard deviation σ is estimated by searching for the tolerance value $\bar{r}$ that minimizes the discrete derivative of $r \to \mathrm{ApEn}(\{y_n(\varepsilon)\}_{n=1}^{N}, m, r) + \log r$. Finally, select a neighborhood $I(\bar{r})$ around $\bar{r}$ and determine the best fit $\bar{\sigma}$ for the function $\sigma \to \mathrm{ApEn}(\{y_n(\varepsilon)\}_{n=1}^{N}, m, r) + \log\left[r/(\sigma\sqrt{\pi})\right]$. Absolute noise estimates are standardized with respect to time series range. An appropriate selection for $I(\bar{r})$ could be $I(\bar{r}) = [r_{max}, \bar{r}]$, where r_{max} represents the tolerance value at which $r \to \mathrm{ApEn}(X, m, r)$ attains its peak value (Scarciglia et al., 2023b).

In this work, the intrinsic brain noise estimation has been performed with embedding dimension $m = 2$, and $\Delta_r = 0.001 \times \{\text{time series range}\}$. These choices are motivated by the method validation on autoregressive models and nonlinear maps (Scarciglia et al., 2023b,a).

2.3. Mean field variability index

We compare the proposed noise estimation algorithm with the Mean Field Variability Index (MFVI), as proposed in Sheppard et al. (2013), which quantifies cerebral activity in terms of synchronization of neuronal interactions. We applied this quantifier to the fMRI series to examine whether the MFVI correlates with aging or if the potential varying levels of noise indicate symptoms of synchrony, asynchrony, or intermittency in the neural networks.

2.4. Experimental data

This study received approval from the University of Pisa's Committee of Bioethics under review number 19/2021 and adhered to the principles outlined in the Declaration of Helsinki. We conducted experiments using two distinct fMRI datasets to assess the generalizability and reliability of our proposed estimation framework. Firstly, we utilized data from the Cam-CAN dataset to evaluate intrinsic brain noise in region of interest (ROI)-based fMRI time series across the adult lifespan. Secondly, we examined the distribution of intrinsic brain noise from the HCP dataset in two experimental conditions to provide an independent and large-sample cohort. These conditions included: (i) ROI-based fMRI time series that matched the setup of the Cam-CAN dataset, and (ii) fMRI data grouped using Independent Component Analysis (ICA).

By analyzing these datasets, we aimed to validate the brain noise modulation and explore the role of brain noise in aggregated data. The inclusion of both ROI-based and ICA-based approaches allows us to gain a comprehensive understanding of intrinsic brain noise across different analysis methods and experimental conditions.

2.4.1. Synthetic time series

While we evaluated the validity of the dynamical noise estimation method on both linear and nonlinear periodic and chaotic maps (Scarciglia et al., 2023b,a), here we evaluate the validity of the noise estimation algorithm on noisy synthetic fMRI series. We simulated an fMRI signal based on the model proposed in Glover (1999). According to this model, the fMRI time series is generated by convolving the hemodynamic response function (HRF) with a stimulus, represented as a series of events occurring at random time points. The HRF itself is modeled as the difference of two gamma functions. To introduce the effects of dynamical noise, we incorporated a sequence of stochastic random variables with a normal distribution $\mathcal{N}(0,\sigma)$ into the HRF.

We conducted two types of simulations on synthetic fMRI data. In the first simulation (Dataset 1), we generated 100 different noisy fMRI series, each comprising $N = 261$ samples and time between two consecutive volumes in the fMRI acquisition, i.e. the repetition time (TR), was set at 1970 ms. The series length and TR were selected in accordance with the Cam-CAN dataset. The dynamical noise was added with a mean of 0 and standard deviation σ, which ranged from $\{0.1, 0.5, 1, 1.5, 2\}$. An exogenous stimulus of 2s duration was also considered. In the second simulation set (Dataset 2), the series length and TR were adjusted to 1200 and 0.72 ms, respectively, aiming to replicate the characteristic fMRI series of the HCP-1200 Connectome dataset. All estimations were performed by setting an embedding dimension of $m = 2$ and a radius resolution of $\Delta_r = 0.001 \times \{\text{time series range}\}$.

2.4.2. Cam-CAN data set description

The dataset consists of multimodal fMRI series collected from a large (approximately N=700), cross-sectional adult lifespan (18–87 years old) population-based sample. The study aimed to characterize age-related changes in cognition and brain structure and function and to uncover the neurocognitive mechanisms that support healthy cognitive aging. For each subject, fMRI recordings in three functional runs (resting state with a repetition time, TR, of 1970 ms, movie-watching with a TR of 2470 ms, and a sensorimotor task with a TR of 1970 ms) were collected. In a subsequent stage, fMRI data were preprocessed and regrouped into 116 ROI series according to the Automated Anatomical Labeling (AAL)1 atlas (Geerligs et al., 2016).

In the present study, we include data from 645 subjects who have completed fMRI series for resting state task. Each fMRI series contains N=216 samples for each ROI, for every subject. Therefore, for each subject, we estimate intrinsic brain noise in 116 ROI-wise fMRI series. Further details on the data collection and characteristics can be found in Taylor et al. (2017).

2.4.3. HCP1200 dataset — Region of interest

We utilized publicly available data from the Human Connectome Project (HCP), which includes a total of 1086 subjects. The data can be accessed at https://www.humanconnectomeproject.org. In our analysis, we specifically focused on the 116 fMRI node time series that correspond to the 116 ROI, as defined by the AAL1 atlas (Geerligs et al., 2016) — consistently with the Cam-CAN setup. The HCP dataset consists of fMRI recordings obtained from two resting-state sessions (Rest1 and Rest2). Each session involved scanning from left to right (LR) and from right to left (RL), resulting in a total of four fMRI

recordings for each subject. Each ROI fMRI time series comprised 1200 volumes, with a repetition time (TR) of 720 ms. This equates to approximately 15 min of scanning for each of the four experimental settings.

2.5. HCP1200 dataset — Nodes

We conducted additional analysis on the HCP dataset, which involved 25 fMRI node time series obtained from each subject. These node time series corresponded to the 25 components resulting from the group-ICA decomposition. Each node time series consisted of $N = 1200$ samples from four resting-state fMRI runs. The HCP consortium performed preprocessing on the 15-minute resting-state fMRI data of each subject, employing a combination of FSL Multivariate Exploratory Linear Optimized Decomposition into Independent Components (MELODIC) (ICA) and FMRIB's ICA-based X-noisifier (FIX) to remove artifacts. Inter-subject registration of the cerebral cortex was accomplished using areal-feature-based alignment and the Multimodal Surface Matching algorithm. For the input of group principal component analysis (PCA), each dataset underwent temporal demeaning and variance normalization. Specifically, the HCP consortium utilized Multivariate Imputation of Gaussian Process (MIGP) group-PCA output as input for FSL's MELODIC tool for group-ICA, applying spatial-ICA at various dimensionalities. For our analysis, we selected a dimensionality of 25, which determined the number of distinct ICA components retained for further investigation. Spatial-ICA was conducted in grayordinate space, encompassing surface vertices as well as subcortical grey matter voxels. The set of ICA spatial maps was then projected onto each subject's fMRI time series data to derive one representative time series per ICA component (referred to as a network "node" in our study). We estimated the noise level for each of the 25 components in each run, and then retained the average across the four runs for subsequent statistical analysis.

3. Results

3.1. Synthetic data

Results are summarized in the boxplots depicted in the subsequent figures, where the red lines represent the median noise standard deviation observed among realizations, and the lower and upper boundaries of the blue boxes indicate the 25th and 75th percentiles of the distribution.

Indeed, results indicate that our approach effectively discriminates between various levels of superimposed noise; there is a direct correlation between the noise intensity and the dispersion around the median value. Notably, the standard deviation of the HRF superimposed noise aligns closely with the one estimated in the synthetic fMRI signal. Nonetheless, the two datasets exhibit some differences. Specifically, estimated noise values seem to be underestimated in the first dataset (refer to Fig. 1(a)), while in the second dataset, they appear to be more accurate (Fig. 1(b)). We believe these differences are primarily due to the varying series lengths; indeed, the longer the series, the more precise the estimation of the noise levels, as previously discussed in Scarciglia et al. (2023a). To address this limitation, we consistently conducted separate analyses for each dataset. It is important to note that the positive trends observed within the two datasets are independent of each other.

3.2. ROI-wise intrinsic brain noise across adult lifespan — CamCAN dataset

For the Cam-CAN dataset, we calculated the Spearman correlation coefficient between the estimated noise power to signal ratio and subjects' age for each ROI. Intrinsic brain noise power in these fMRI series reaches up to the power of the signal and varies among brain areas and age. To illustrate, in Fig. 2 the ROIs showing a significant

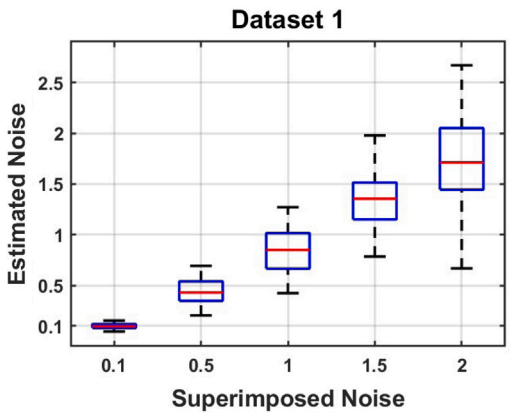

(a) Superimposed versus estimated noise in synthetic series from Dataset 1. The series consist of $N = 261$ samples and a TR of 1970 ms, simulating characteristic series of the Cam-CAN dataset.

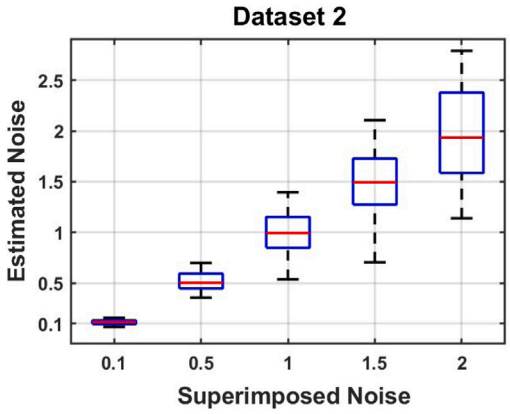

(b) Superimposed versus estimated noise in synthetic series from Dataset 2. The series consist of $N = 1200$ samples and a TR of 720 ms, simulating characteristic series of the HCP-1200 dataset.

Fig. 1. Noise estimates in synthetic data: For each superimposed noise level (x-axis), noise was estimated using $m = 2$ and $\Delta r = 0.001 \times \{\text{time series range}\}$ on 100 realizations of the noisy synthetic fMRI model.

correlation between noise and age are represented. From the dark red areas, we note that the correlations are mostly verified in the precentral and frontal areas. More details about Spearman correlation coefficient and associated p-value for any ROI between subject-wise noise estimates and subjects' ages, alongside the AAL1 reference abbreviation and corresponding MNI coordinates are provided in Table A1 of the Appendix.

A total of 73 ROIs exhibit statistically significant positive correlations between noise and age, while only two ROIs (# 71 and # 72) show a significant, negative trend. The left-hand side column of Fig. 3 displays exemplary ROI statistics (#12=Frontal Inferior Operculum R, #14=Triangular Inferior Frontal Gyrus R, and #16=Frontal Inferior Orbit R) with statistically significant Spearman correlation coefficients ($\rho = 0.2843$, 0.2763, and 0.2573, respectively) and $p < (0.05/116)$ computed subject-wise, following a Bonferroni correction. It is noteworthy that intrinsic brain noise can contribute substantially to the overall signal power, ranging from 10% to 100% of the fMRI signal power. In addition, we found that the estimated brain noise levels positively correlate with the fMRI signal power for any ROI, with a mean $\pm$ standard deviation correlation coefficient of 0.66 ± 0.078 among all the ROIs, indicating that the brain noise significantly contribute the fMRI signal variability. The detailed results can be found in Table A2(a) of the Supplementary Material.

The MFVI index does not correlate with the estimated noise variance, nor with aging. The MFVI values are consistently slightly below

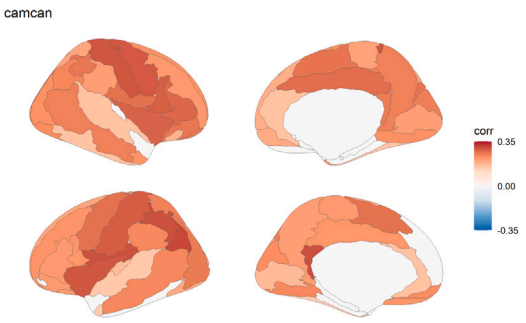

Fig. 2. Brain ROIs with a significant correlation between noise and age. The brain images depict the first 78 ROIs (excluding the limbic system, cerebellum, and vermis), illustrating the significant Spearman correlation coefficients between noise and aging. These images correspond to the Cam-CAN dataset, where darker regions indicate stronger correlations.

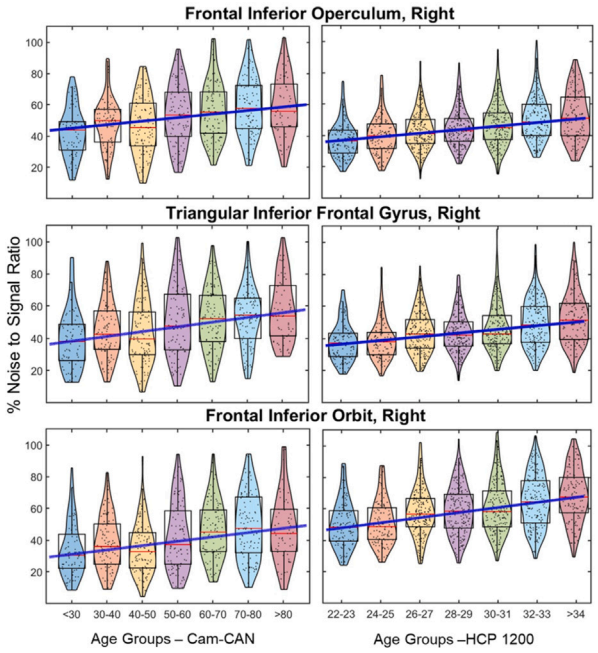

Fig. 3. Age-Related fMRI Noise Variation in Key ROIs within the Cam-CAN and HCP 1200 Datasets. The figure presents boxplot statistics of the noise to signal ratio, computed as the variance of the encountered noise divided by the power of the signal, for three significant regions of interest (ROIs): Frontal Inferior Operculum R (#12), Triangular Inferior Frontal Gyrus R (#14), and Frontal Inferior Orbit R (#16). The left-hand column corresponds to the Cam-CAN dataset, while the right-hand column represents the first recording of the four HCP-1200 trials. In the left-hand side panels, the figure shows the variations in noise to signal ratio across different age groups (18–87) for the Cam-CAN dataset. The age groups are categorized as follows: <30 (73 subjects), 30–40 (95 subjects), 40–50 (110 subjects), 50–60 (95 subjects), 60–70 (104 subjects), 70–80 (107 subjects), and > 80 (61 subjects). Individual subject noise estimations are denoted by black crosses. All the ROIs exhibit a significant positive trend in median noise levels as age increases, with Spearman coefficients of $\rho = 0.9286$, 0.9286, and 0.87 (p=0.0067, 0.0067, and 0.0238, respectively). Similarly, the right-hand side panels illustrate the relationship between the noise to signal ratio and age range series for the first recording of the HCP-1200 trials. The age groups are divided as follows: 22–23 (114 subjects), 24–25 (113 subjects), 26–27 (195 subjects), 28–29 (185 subjects), 30–31 (177 subjects), 32–33 (177 subjects), and > 34 (121 subjects). In this case as well, the boxplots demonstrate significant positive trends in median noise levels as age increases, with Spearman coefficients of $\rho = 1.000$, 0.8929, and 0.9643 (p<0.0123). Across all panels, the thick blue line represents the least-square linear regression of the group-wise median noise levels.

the threshold of 0.215, indicating partial phase synchronization of the underlying neuronal activity.

Table 1
Percentages of ROIs with consistent correlation among the different recordings of HCP - 1200.

Percentages of Matches	HCP_REST1_LR	HCP_REST1_RL	HCP_REST2_LR	HCP_REST2_RL
HCP_REST1_LR	100,00%	89,66%	93,10%	93,10%
HCP_REST1_RL	89,66%	100,00%	89,66%	86,21%
HCP_REST2_LR	93,10%	89,66%	100,00%	91,38%
HCP_REST2_RL	93,10%	86,21%	91,38%	100,00%

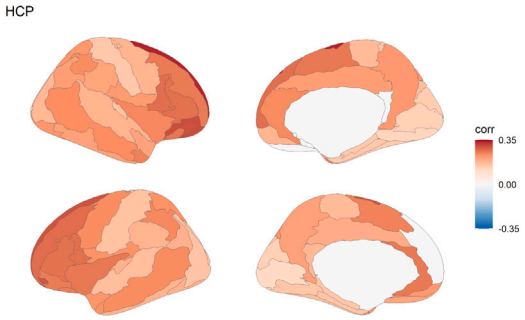

Fig. 4. Brain ROIs with a significant correlation between noise and age. The brain images represent the first 78 ROIs – limbic system, cerebellum and vermis are excluded – where there are represented the significant Spearman correlation coefficient between noise and aging. The upper four brain images are associated with the Cam-CAN dataset; the remaining ones with the HCP-1200 dataset. The darker the areas, the higher are the correlations.

3.3. ROI-wise intrinsic brain noise across adult lifespan — HCP connectome 1200

We conducted noise-to-signal ratio estimations for all four recordings of the HCP dataset across different tasks. Additionally, we calculated the Spearman correlation coefficient between the estimated noise power and the subjects' age for each ROI in all sessions. A matching analysis was conducted to compare results from the four different resting state sessions. A match for a ROI was determined if the noise levels of two different datasets either significantly changed with age (Spearman $p < 0.05/116$) or did not exhibit a joint correlation with age (Spearman $p > 0.05/116$). The results in Table 1 reveal that there were no significant differences in noise levels across the various recordings, with at least 90% of the ROIs displaying matching trends between different resting state sessions.

Therefore, for the sake of brevity and without loss of generality, we provide a further details and analyses on the HCP dataset focusing on the first recording in the resting state, denoted as "Rest1", which was scanned from left to right (LR). Specifically, in Fig. 4 we highlight the Spearman correlation coefficient between the estimated noise power and the subjects' age for each ROI in this particular recording.

Among the 116 ROIs analyzed, 92 of them show statistically significant positive correlations between noise and age. As for the Cam-CAN dataset, Fig. 3 illustrates this relationship, specifically highlighting three ROIs: Frontal Inferior Operculum R (#12), Triangular Inferior Frontal Gyrus R (#14), and Frontal Inferior Orbit R (#16). These ROIs exhibit statistically significant Spearman correlation coefficients (ρ = 0.3276, 0.3027, and 0.328, respectively) with corresponding subject-wise p-values of less than (0.05/116), computed following a Bonferroni correction.

For a comprehensive overview of the Spearman correlation coefficients and associated p-values between subject-wise noise estimates and subjects' ages, please refer to Table A4 in the Appendix. This table provides the results for all ROIs, along with the AAL1 reference abbreviation and corresponding MNI coordinates. Similarly to the previous

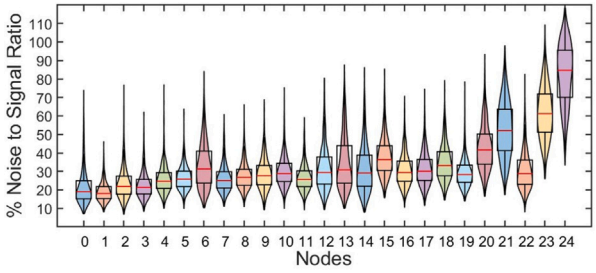

Fig. 5. fMRI Time Series Physiological Noise Analysis. Displayed are the boxplot statistics for each group-ICA component within the HCP1200 dataset, considering an embedding dimension of $m = 2$.

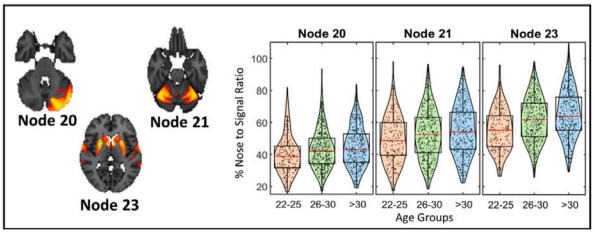

Fig. 6. Age-Related Noise Variation in fMRI Cluster Nodes. This figure illustrates exemplary node-wise noise trends in relation to aging, using an embedding dimension of $m = 2$. Black crosses represent noise estimation for individual subjects, while the horizontal red line signifies the median noise level per age range. Age groups are divided into 22–25 (218 subjects), 25–30 (432 subjects), and > 30 (353 subjects).

analysis, we found positive correlations between estimated brain noise levels and fMRI signal variance, with a mean and standard deviation of 0.85 ± 0.074. This confirms that noise plays a fundamental role in the series variability. The results can be found in Table A2(b) of the Supplementary Material.

Also this case, the MFVI index does not correlate with the estimated noise variance or with aging. The MFVI values are notably slightly above the threshold of 0.215, indicating complex coherence or intermittency in neuronal activity.

3.4. Intrinsic brain noise in aggregated fMRI series

We further conducted noise estimation on fMRI series obtained from 25 highly aggregated nodes. For the purpose of brevity and due to the similarity of the noise estimation across the four recordings in the resting state of the HCP-1200 Dataset, we present the results specifically for the recording in task “Rest1”, scanned from LR. The findings are summarized through group-wise boxplot statistics, as depicted in Fig. 5. The significance level for the test was set at $\alpha = 0.05/25$, considering the Bonferroni correction.

From a spatial perspective, intrinsic brain noise contributes to the entirety of fMRI variance and demonstrates variability across different brain regions or group-ICA clusters. On average, noise levels range from 20% to 40% for most nodes, except for clusters 21, 23, and 24, which exhibit median noise power-to-signal power ratios ranging from 50% to 90%.

From the perspective of aging, we classified the fMRI series and the associated stochastic brain dynamics into three age ranges: 22–25, 26–30, and >30. Across all nodes, we observed a consistent pattern of increasing noise to signal ratios with aging. This increasing trend was confirmed by conducting a Kruskal–Wallis test, where the null hypothesis assumed equal medians among the three age cohorts. Exemplary boxplot statistics for nodes exhibiting higher brain noise and displaying significant noise trends with age are presented in Fig. 6. For more comprehensive information, please refer to Table A5 in the Appendix.

4. Discussion

In this study, we approached fMRI acquisition as a sampled output of an unknown dynamical system representing deterministic and stochastic brain activity, acknowledging that measurement and intrinsic brain noise are inherently interwoven with the observed dynamics. Measurement noise, or additive noise, arises from external sources due to limitations or inaccuracies in the data acquisition process, such as sensor fluctuations, environmental interference, or background noise. This noise directly impacts the recorded signal, often masking the true underlying biological phenomena. In contrast, intrinsic biological noise, or dynamical noise, is an inherent property of biological systems, stemming from the stochastic nature of various biological processes, such as gene expression, cellular activity, or neural fluctuations. Quantifying this dynamical noise is challenging, as it depends on the specific modeling attributed to the deterministic brain activity.

We introduced an estimation framework for the intrinsic brain noise when the underlying deterministic dynamics is unknown. Our method leverages the nonlinear quantifier (ApEn) (Pincus, 1991) and its differential behavior in noisy series when the quantifier is considered as a function of one of its parameters (Scarciglia et al., 2023b). We examined stochastic brain components across brain maturation. Assuming that measurement noise is uncorrelated with aging due to its distribution across data acquisition from various subjects and MRI machines, we discovered a modulation of intrinsic brain noise with age progression in healthy individuals.

Our findings based on the Cam-CAN and HCP Connectome 1200 datasets highlight the distinct distribution of stochastic brain activity components across various brain regions during resting state, as well as the modulation of their power during maturation. The behavior of noise exhibits a similar trend for approximately 80%–85% of the ROIs in both the Cam-CAN and the four recordings of the HCP Connectome. Specifically, almost all the trends demonstrate a statistically significant increase along with aging across various brain regions. Only two ROIs in the Cam-CAN dataset exhibit a negative trend, while the negative trend is not significant in the HCP Connectome dataset, possibly due to the narrower age range considered. Additionally, our analysis suggests that in the reduction of the variability of the fMRI series along with aging (Xie et al., 2020; Grady and Garrett, 2014), the intrinsic stochastic component is predominant in the variability series of elderly subjects, while this noise is marginal in the overall dynamics of the young cohort. From the comparison with the MFVI, we deduce that the intrinsic noise could bias the MFVI, masking the actual interaction of the underlying neuronal activity. We hypothesize that the encountered noise in the BOLD fMRI signals might overshadow the correlated neuronal activity through neurovascular coupling (Hillman, 2014). Confirming the method’s validity on noisy synthetic fMRI signals enhances its resilience to the observed positive trend. Although the series length could introduce bias when comparing different sample series, it is essential to note that the escalating noise level has been independently identified in each dataset. Additional, unreported analyses imply that the amount of noise is approximately linked to the quantity of pairs of temporally close stimuli, based on the employed model for fMRI generation. Furthermore, it is important to note that we performed additional noise estimation analyses, which are not presented here, to validate the robustness of our findings. These analyses included: (i) applying a z-score transformation to each fMRI series; (ii) concatenating the HCP-related z-scored series from different sessions; (iii) cutting the HCP series length to match the length of the CAM-CAN series (261 samples); (iv) resampling the HCP series to align with the CAM-CAN TR by taking one sample every three samples. Notably, these comprehensive analyses produced results that align with those presented in the previous section and supplementary material; in fact, results matching between datasets ranged between 72% and 78%. This concurrence reinforces the reliability and consistency of our findings.

Furthermore, approximately 90% of the significant positive correlations are predominantly observed within the first 90 ROIs. Among all areas, we have identified that frontal regions (in particular, Frontal operculum R, and orbital part of Inferior Frontal gyrus R) are the most correlated regions with the estimated brain noise. Other regions exhibiting high correlations between noise and aging are as the precentral areas, Rolandic Operculum, medial Cingulum and occipital areas. Age-dependent modulation of fMRI noise is consistently demonstrated through ICA spatial clusters and standard ROIs in two distinct, publicly available datasets with pre-processed data. In the HCP fMRI dataset, despite the narrow age range, the significant number of subjects and the widespread availability of literature on such data support its use for investigating brain noise. We remark that while the spatial clustering in ICA can be viewed as a denoising method, the noise identified in these processed series is dynamic and inherently linked to the intrinsic brain dynamics, making its removal a challenging task.

The presence of noise can differentially influence biomarker definition and estimation across distinct brain regions, possibly resulting in inaccuracies in pinpointing and characterizing trustworthy indicators for specific conditions. Consequently, these inaccuracies may give rise to misinterpretations and incorrect clinical decisions, particularly when comparing biomarker levels among different brain areas. Therefore, precise estimation of biological noise is crucial for evaluating psychological function and associated pathophysiology. Among all the possible applications, our method could enhance the performances of existing methods for classifying EEG series, like the mean-field variability index (Sheppard et al., 2013), by quantifying how much the index is biased by the amount of noise.

Note that our proposed noise estimation framework can be applied to any time series, making it potentially valuable in fields beyond computational physiology and neuroscience.

CRediT authorship contribution statement

Andrea Scarciglia: Writing – review & editing, Writing – original draft, Visualization, Validation, Software, Methodology, Investigation, Formal analysis, Data curation, Conceptualization. **Vincenzo Catrambone:** Writing – review & editing, Writing – original draft, Visualization, Software, Data curation. **Martina Bianco:** Writing – review & editing, Data curation. **Claudio Bonanno:** Writing – review & editing, Writing – original draft, Supervision, Methodology, Funding acquisition, Conceptualization. **Nicola Toschi:** Writing – review & editing, Writing – original draft, Visualization, Software, Data curation. **Gaetano Valenza:** Writing – review & editing, Writing – original draft, Supervision, Methodology, Funding acquisition, Conceptualization.

Declaration of competing interest

The authors declare that they have no known competing financial interests or personal relationships that could have appeared to influence the work reported in this paper.

Data availability

The Human Connectome Data used for this study are publicly available at: http://www.humanconnectomeproject.org

TheCam-CAN Data used for this study are publicly available at: https://camcan-archive.mrc-cbu.cam.ac.uk/dataaccess/

The software code to compute the brain noise estimation is available at: https://github.com/AndScar/noise_estimation

Acknowledgments

The research leading to these results has received partial funding by the European Commission Horizon 2020 research and innovation programme under grant agreement No. 101017727 of the project EXPERIENCE; by the Italian Ministry of Education and Research (MIUR) in the framework of the FoReLab project (Departments of Excellence); by #NEXTGENERATIONEU (NGEU) and funded by the Ministry of University and Research (MUR), National Recovery and Resilience Plan (NRRP), project MNESYS (PE0000006) (to NT)– A Multiscale integrated approach to the study of the nervous system in health and disease (DN. 1553 11.10.2022); by the MUR-PNRR M4C2I1.3 PE6 project PE00000019 Heal Italia (to NT); by the NATIONAL CENTRE FOR HPC, BIG DATA AND QUANTUM COMPUTING, within the spoke "Multiscale Modeling and Engineering Applications" (to NT).

Appendix A. Supplementary data

Supplementary material related to this article can be found online at https://doi.org/10.1016/j.neuroimage.2024.120562.

References

Basalyga, G., Salinas, E., 2006. When response variability increases neural network robustness to synaptic noise. Neural Comput. 18 (6), 1349–1379.

Birn, R.M., Smith, M.A., Jones, T.B., Bandettini, P.A., 2006. Separating respiratory-variation-related fluctuations from neuronal-activity-related fluctuations in fMRI. Neuroimage 31 (4), 1536–1548.

Branco, T., Staras, K., 2009. The probability of neurotransmitter release: Variability and feedback control at single synapses. Nat. Rev. Neurosci. 10 (5), 373–383.

Cabeza, R., 2002. Hemispheric asymmetry reduction in older adults: the HAROLD model. Psychol. Aging 17 (1), 85.

Chen, J.J., 2019. Functional MRI of brain physiology in aging and neurodegenerative diseases. Neuroimage 187, 209–225.

Chen, J.J., Rosas, H.D., Salat, D.H., 2013. The relationship between cortical blood flow and sub-cortical white-matter health across the adult age span. PLoS One 8 (2), e56733.

Daselaar, S.M., Fleck, M.S., Dobbins, I.G., Madden, D.J., Cabeza, R., 2006. Effects of healthy aging on hippocampal and rhinal memory functions: An event-related fMRI study. Cerebral Cortex 16 (12), 1771–1782.

Deco, G., Jirsa, V., McIntosh, A.R., Sporns, O., Kötter, R., 2009a. Key role of coupling, delay, and noise in resting brain fluctuations. Proc. Natl. Acad. Sci. 106 (25), 10302–10307.

Deco, G., Rolls, E.T., Romo, R., 2009b. Stochastic dynamics as a principle of brain function. Progress Neurobiol. 88 (1), 1–16.

Dennis, E.L., Thompson, P.M., 2014. Functional brain connectivity using fMRI in aging and Alzheimer's disease. Neuropsychol. Rev. 24, 49–62.

Destexhe, A., Contreras, D., 2006. Neuronal computations with stochastic network states. Science 314 (5796), 85–90.

Fox, M.D., Raichle, M.E., Snyder, A.Z., 2007. Non-invasive source localization and imaging of neuronal activity with magnetoencephalography. Int. Congress Ser. 1300, 225–228.

Fox, M.D., Snyder, A.Z., Vincent, J.L., Corbetta, M., Van Essen, D.C., Raichle, M.E., 2005. The human brain is intrinsically organized into dynamic, anticorrelated functional networks. Proc. Natl. Acad. Sci. 102 (27), 9673–9678.

Geerligs, L., Henson, R.N., et al., 2016. Functional connectivity and structural covariance between regions of interest can be measured more accurately using multivariate distance correlation. NeuroImage 135, 16–31.

Glover, G.H., 1999. Deconvolution of impulse response in event-related BOLD fMRI1. Neuroimage 9 (4), 416–429.

Grady, C.L., Garrett, D.D., 2014. Understanding variability in the BOLD signal and why it matters for aging. Brain Imaging Behav. 8, 274–283.

Grady, C.L., McIntosh, A.R., Craik, F.I., 2000. Age-related reductions in human recognition memory due to impaired encoding. Science 289 (5479), 606–608.

Heffernan, K.S., Jae, S.Y., Lee, M., Woods, J.A., Fernhall, B., 2008. Arterial wave reflection and vascular autonomic modulation in young and older men. Aging Clin. Exp. Res. 20, 1–7.

Hillman, E.M., 2014. Coupling mechanism and significance of the BOLD signal: A status report. Annu. Rev. Neurosci. 37, 161–181.

Hoffman, C., Cheng, J., Ji, D., Dabaghian, Y., 2023. Pattern dynamics and stochasticity of the brain rhythms. Proc. Natl. Acad. Sci. 120 (14), e2218245120.

Krüger, G., Glover, G.H., 2001. Physiological noise in oxygenation-sensitive magnetic resonance imaging. Magn. Reson. Med. 46 (4), 631–637.

Lavanga, M., Stumme, J., Yalcinkaya, B.H., Fousek, J., Jockwitz, C., Sheheitli, H., Bittner, N., Hashemi, M., Petkoski, S., Caspers, S., et al., 2023. The virtual aging brain: Causal inference supports interhemispheric dedifferentiation in healthy aging. NeuroImage 283, 120403.

Liu, T.T., 2016. Noise contributions to the fMRI signal: An overview. NeuroImage 143, 141–151.

Lowe, M.J., Mock, B.J., Sorenson, J.A., 1998. Functional connectivity in single and multislice echoplanar imaging using resting-state fluctuations. NeuroImage 7 (2), 119–132.

Lu, H., Xu, F., Rodrigue, K.M., Kennedy, K.M., Cheng, Y., Flicker, B., Hebrank, A.C., Uh, J., Park, D.C., 2011. Alterations in cerebral metabolic rate and blood supply across the adult lifespan. Cerebral Cortex 21 (6), 1426–1434.

MacDonald, M.E., Pike, G.B., 2021. MRI of healthy brain aging: A review. NMR Biomed. 34 (9), e4564.

Marstaller, L., Williams, M., Rich, A., Savage, G., Burianová, H., 2015. Aging and large-scale functional networks: White matter integrity, gray matter volume, and functional connectivity in the resting state. Neuroscience 290, 369–378.

McDonnell, M.D., Ward, L.M., 2011. The benefits of noise in neural systems: Bridging theory and experiment. Nat. Rev. Neurosci. 12 (7), 415–425.

Park, D.C., Polk, T.A., Park, R., Minear, M., Savage, A., Smith, M.R., 2004. Aging reduces neural specialization in ventral visual cortex. Proc. Natl. Acad. Sci. 101 (35), 13091–13095.

Petkoski, S., Ritter, P., Jirsa, V.K., 2023. White-matter degradation and dynamical compensation support age-related functional alterations in human brain. Cerebral Cortex 33 (10), 6241–6256.

Pincus, S.M., 1991. Approximate entropy as a measure of system complexity. Proc. Natl. Acad. Sci. 88 (6), 2297–2301.

Ponce-Alvarez, A., Jouary, A., Privat, M., Deco, G., Sumbre, G., 2018. Whole-brain neuronal activity displays crackling noise dynamics. Neuron 100 (6), 1446–1459.

Power, J.D., Barnes, K.A., Snyder, A.Z., Schlaggar, B.L., Petersen, S.E., 2012. Spurious but systematic correlations in functional connectivity MRI networks arise from subject motion. Neuroimage 59 (3), 2142–2154.

Reuter-Lorenz, P.A., Stanczak, L., 2000. Compensatory encoding in the aging brain: A functional magnetic resonance imaging study. Neuroreport 11 (17), 3785–3790.

Scarciglia, A., Catrambone, V., Bonanno, C., Valenza, G., 2023a. Physiological noise: Definition, estimation, and characterization in complex biomedical signals. IEEE Trans. Biomed. Eng..

Scarciglia, A., Gini, F., Catrambone, V., Bonanno, C., Valenza, G., 2023b. Estimation of dynamical noise power in unknown systems. IEEE Signal Process. Lett..

Sheppard, L., Hale, A., Petkoski, S., McClintock, P., Stefanovska, A., 2013. Characterizing an ensemble of interacting oscillators: The mean-field variability index. Phys. Rev. E 87 (1), 012905.

Tarumi, T., Khan, M.A., Liu, J., Tseng, B.M., Parker, R., Riley, J., Tinajero, C., Zhang, R., 2014. Cerebral hemodynamics in normal aging: Central artery stiffness, wave reflection, and pressure pulsatility. J. Cereb. Blood Flow Metab. 34 (6), 971–978.

Taylor, J.R., Williams, N., Cusack, R., Auer, T., Shafto, M.A., Dixon, M., Tyler, L.K., Henson, R.N., et al., 2017. The cambridge centre for ageing and neuroscience (Cam-CAN) data repository: Structural and functional MRI, MEG, and cognitive data from a cross-sectional adult lifespan sample. NeuroImage 144, 262–269.

Thomas, B.P., Liu, P., Park, D.C., Van Osch, M.J., Lu, H., 2014. Cerebrovascular reactivity in the brain white matter: Magnitude, temporal characteristics, and age effects. J. Cereb. Blood Flow Metabol. 34 (2), 242–247.

Van Essen, D.C., Smith, S.M., Barch, D.M., Behrens, T.E., Yacoub, E., Ugurbil, K., 2013. The WU-Minn human connectome project: An overview. Neuroimage 80, 62–79.

Xekardaki, A., Rodriguez, C., Montandon, M.-L., Toma, S., Tombeur, E., Herrmann, F.R., Zekry, D., Lovblad, K.-O., Barkhof, F., Giannakopoulos, P., et al., 2015. Arterial spin labeling may contribute to the prediction of cognitive deterioration in healthy elderly individuals. Radiology 274 (2), 490–499.

Xie, W., Peng, C.-K., Shen, J., Lin, C.-P., Tsai, S.-J., Wang, S., Chu, Q., Yang, A.C., 2020. Age-related changes in the association of resting-state fMRI signal variability and global functional connectivity in non-demented healthy people. Psychiatry Res. 291, 113257.